OPTIMUM LAYOUTS FOR WIRE-ACTUATED PARALLEL MANIPULATORS CONSIDERING THEIR STIFFNESS CHARACTERISTICS AND WIRE FAILURE

Leila Notash, Amir Moradi
Department of Mechanical and Materials Engineering, Queen's University, Kingston, Ontario Canada
Email: notash@me.queensu.ca

Received April 2012, Accepted September 2012
No. 12-CSME-52, E.I.C. Accession 3372

ABSTRACT

In this paper, stiffness of planar translational wire-actuated parallel manipulators is studied. The complete form of the stiffness matrix of the two degrees of freedom manipulators is formulated parametrically. The differential form of the static force balance equations is used to incorporate the variation of wire stiffness with wire length and the change in the Jacobian matrix under external force in the stiffness model. Failure of a wire, for the cases that the wire is disconnected or slack, as well as reconfiguring the anchor positions are investigated and their effects on the workspace of manipulators are presented while satisfying the constraints on wire tension and minimum stiffness. The stiffness characteristics of an example manipulator, before and after a wire failure, are discussed. Optimum layouts of the manipulator, by reconfiguring the positions of wire anchors, are identified to maximize the area of the stiffness maps.

Keywords: wire-actuated parallel manipulators; stiffness map; failure analysis; optimum layout.

CONFIGURATION OPTIMALE DE MANIPULATEURS PARALLÈLES ACTIONNÉS PAR CÂBLES EN CONSIDÉRANT LEUR CARACTÉRISTIQUE DE RIGIDITÉ ET DE DÉFAILLANCE DES CÂBLES

RÉSUMÉ

Dans cet article, on étudie la rigidité des manipulateurs parallèles plans de translation actionnés par câbles. La forme complète de la matrice de rigidité des manipulateurs à deux degrés de liberté est formulée sur un plan paramétrique. La forme différentielle des équations des forces statiques est utilisée pour incorporer les variations de la rigidité du câble avec la longueur du câble et le changement de la matrice jacobienne soumise à forces externes dans le modèle de rigidité. La défaillance d'un câble, pour les cas où le câble serait déconnecté ou détendu, de même que la reconfiguration des positions d'ancrage sont étudiées. Les effets sur l'espace de travail des manipulateurs sont présentés pour satisfaire les contraintes de tension du câble et de rigidité minimale. Les caractéristiques de rigidité d'un manipulateur modèle, avant et après la défaillance, sont discutées. Les configurations optimales du manipulateur par reconfiguration des positions des ancrages de câbles, sont identifiées pour maximiser l'aire des cartes de rigidité.

Mots-clés : manipulateurs parallèles actionnés par câbles; cartes de rigidité; analyse de défaillance; configuration optimale.

1. INTRODUCTION

In this paper planar wire-actuated parallel manipulators with two degrees of freedom (DOF) are considered, in which the mobile platform is attached to the base with multiple wires. The light weight of wire actuators and easy assembly/disassembly and transportation of these manipulators are some of their advantages. Wires can be used only when they are in tension. Thus, keeping the positive tension in wires is a challenge. Therefore, in the absence of gravity and external wrench (force/moment), at least $n+1$ wires are required in the design of a fully controllable n DOF manipulator. Because of wires, the stiffness of wire-actuated manipulators is relatively low, hence stiffness analysis is necessary.

The stiffness of manipulators can be used as an index of the accuracy in the static case at the position and force levels, and for optimum design of manipulators. Stiffness matrix transforms a differential displacement of the end effector of a manipulator into the corresponding incremental change in the applied force and moment on its end effector. Stiffness matrix of manipulators is symmetric when it is formulated with respect to a reference frame which is located at the end effector and has the orientation of the fixed base frame and the application point of the external forces are coincident with the origin of this reference frame [1–4]. The symmetry or asymmetry of the stiffness matrix of manipulators under external loading was investigated in [5–7]. The design of a wire-actuated manipulator for ultrahigh speed motion was studied in [8] based on stiffness analysis. In [9], the optimum design of the 3 DOF spherical parallel manipulators based on the conditioning and stiffness indices was studied, and a conceptual design of variable stiffness elements using wire-actuated mechanisms was presented in [10].

In [11], the mechanical failures of parallel and serial manipulators were presented and classified. A failure recovery methodology for wire-actuated parallel manipulators was presented in [12]. In [13], the effect of failure of a wire on stiffness maps of planar wire-actuated parallel manipulators was investigated.

Knowledge of optimum layout of a manipulator can be used in design and control of the manipulator. For instance, the lost stiffness of wire-actuated parallel manipulators after failure of a wire can be retrieved partially by changing the anchor positions of the manipulator. The optimum layouts of 2 DOF planar wire-actuated manipulators are introduced in this paper, i.e. optimum anchor positions are identified to maximize the manipulator workspace with required minimum stiffness (area of the stiffness map) before and after failure. The stiffness modelling and wire failure, when a wire is slack or disconnected, are presented in Section 2. The stiffness maps for a three-wire manipulator before and after the failure are developed in Section 3 and the optimum layouts of the manipulator are introduced. The conclusions of article are in Section 4.

2. MODELLING

The parameters and reference frame of the planar translational wire-actuated parallel manipulators, in which the mobile platform is a point mass, are depicted in Fig. 1. Coordinate system $\Psi(X,Y)$ is attached to the base at point 0. The wire is released from a spool attached to an electric motor. To ensure a non-zero minimum length for each wire, a pulley is placed at anchor points A_i between the spool of wire i and its attachment point on the mobile platform as shown in Fig. 1. The wire lengths between the motor spool and the pulley and between the pulley and the attachment point on the mobile platform are, respectively, denoted as l_{ci} and l_i. Given the position vector of the mobile platform $\mathbf{p} = [p_x \;\; p_y]^T$ and the position vector of anchor A_i, $\mathbf{a}_i = [a_{ix} \quad a_{iy}]^T$, i =1, …, n, wire orientation α_i and wire length l_i are formulated using the inverse displacement analysis as:

$$l_i = \sqrt{(a_{ix}-p_x)^2 + (a_{iy}-p_y)^2}\,, \tag{1}$$

$$\alpha_i = \text{atan2}\ (a_{iy}-p_y, a_{ix}-p_x)\,. \tag{2}$$

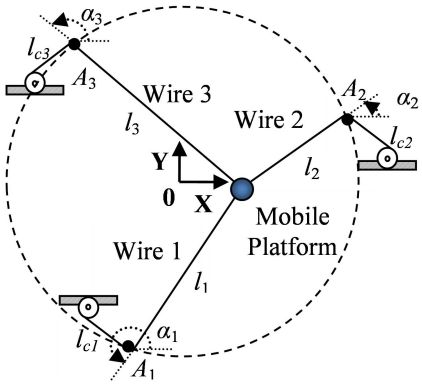

Fig. 1. Coordinate system and variables of 2 DOF planar three-wire-actuated parallel manipulators.

The static force balance for the manipulator can be written as:

$$\mathbf{F} = \mathbf{J}^T \boldsymbol{\tau}, \tag{3}$$

where vector $\mathbf{F} = [F_x \quad (F_y - mg)]^T$ corresponds to the Cartesian forces (wrench) applied on the mobile platform and $\boldsymbol{\tau} = [\tau_1 \ \cdots \ \tau_n]^T$ is the $n \times 1$ vector of wire tensions. The $2 \times n$ transposed Jacobian matrix of the manipulator in terms of the wire orientations α_i is:

$$\mathbf{J}^T = [\mathbf{J}_1^T \cdots \mathbf{J}_n^T] = -\begin{bmatrix} \cos\alpha_1 & \cdots & \cos\alpha_n \\ \sin\alpha_1 & \cdots & \sin\alpha_n \end{bmatrix}, \tag{4}$$

where $\cos\alpha_i = \frac{(a_{ix} - p_x)}{l_i}$ and $\sin\alpha_i = \frac{(a_{iy} - p_y)}{l_i}$. The non-negative wire tensions in terms of wrench $\mathbf{F}$ and generalized (Moore-Penrose) inverse of the transposed Jacobian matrix $\mathbf{J}^T$, $\mathbf{J}^{\#T}$, are calculated using:

$$\boldsymbol{\tau} = \boldsymbol{\tau}_p + \boldsymbol{\tau}_h = \mathbf{J}^{\#T}\mathbf{F} + \mathbf{N}\boldsymbol{\lambda}, \tag{5}$$

where $\boldsymbol{\tau}_p = \mathbf{J}^{\#T}\mathbf{F}$ is the minimum norm solution, and $\boldsymbol{\tau}_h = \mathbf{N}\boldsymbol{\lambda}$ is the homogeneous solution in which the columns of the $n \times (n-m)$ matrix $\mathbf{N}$ correspond to the orthonormal basis of the null space of $\mathbf{J}^T$ and $\boldsymbol{\lambda}$ is an $(n-m) \times 1$ arbitrary vector.

2.1. Stiffness matrix

To calculate the stiffness matrix, Eq. (3) is differentiated as:

$$\delta\mathbf{F} = \delta\mathbf{J}^T\boldsymbol{\tau} + \mathbf{J}^T\delta\boldsymbol{\tau}. \tag{6}$$

Then, the stiffness matrix $\mathbf{K}$ can be formulated by re-arranging Eq. (6) as:

$$\delta\mathbf{F} = \mathbf{K}\,\delta\mathbf{p}. \tag{7}$$

Column i of matrix $\mathbf{J}^T$ is expressed in terms of the corresponding wire orientation α_i. Hence, the first term on the right-hand side of Eq. (6) can be expanded as:

$$\delta\mathbf{J}^T\boldsymbol{\tau} = \sum_{i=1}^{n} \delta\mathbf{J}_i^T \tau_i = \sum_{i=1}^{n} \left(\frac{\partial \mathbf{J}_i^T}{\partial \alpha_i}\delta\alpha_i\right)\tau_i. \tag{8}$$

A relationship between the differential of wire orientations $\delta\boldsymbol{\alpha} = [\delta\alpha_1 ... \delta\alpha_n]^T$ and the platform twist could also be derived. The mobile platform position in terms of the parameters of wire i, $i = 1, \ldots, n$, can be written as:

$$\mathbf{p} = \begin{bmatrix} p_x \\ p_y \end{bmatrix} = \begin{bmatrix} a_{i_x} - l_i \cos\alpha_i \\ a_{i_y} - l_i \sin\alpha_i \end{bmatrix}. \tag{9}$$

Differentiating Eq. (9), a relationship between the vector of differential wire orientations $\delta\boldsymbol{\alpha} = [\delta\alpha_1 ... \delta\alpha_n]^T$ and the twist $\delta\mathbf{p} = [\delta p_x \;\; \delta p_y]^T$ is derived as:

$$\delta\boldsymbol{\alpha} = \begin{bmatrix} \frac{\sin\alpha_1}{l_1} & -\frac{\cos\alpha_1}{l_1} \\ \vdots & \vdots \\ \frac{\sin\alpha_n}{l_n} & -\frac{\cos\alpha_n}{l_n} \end{bmatrix} \begin{bmatrix} \delta p_x \\ \delta p_y \end{bmatrix} = \mathbf{A}\delta\mathbf{p}. \tag{10}$$

Considering the transposed Jacobian matrix in Eq. (4), $\delta\mathbf{J}_i^T$ can be written in terms of $\delta\mathbf{p}$ as:

$$\delta\mathbf{J}_i^T = \begin{bmatrix} 0 & \cdots & \sin\alpha_i & \cdots & 0 \\ 0 & \cdots & -\cos\alpha_i & \cdots & 0 \end{bmatrix} \mathbf{A}\delta\mathbf{p}. \tag{11}$$

For wire-actuated parallel manipulators, the stiffness of each wire is modelled as a simple linear spring. Thus, to formulate the second term on the right-hand side of Eq. (6), the changes in wire forces is written as:

$$\delta\boldsymbol{\tau} = \mathbf{K}_q\delta\mathbf{l}, \tag{12}$$

where the diagonal wire stiffness matrix in terms of the stiffness constant of wire actuator i, k_i, is:

$$\mathbf{K}_q = diag[k_1 \cdots k_n]. \tag{13}$$

The differential form of twist is related to the vector of differential change in wire lengths $\delta\mathbf{l} = [\delta l_1 ... \; \delta l_n]^T$ by the Jacobian matrix as:

$$\delta\mathbf{l} = \mathbf{J}\,\delta\mathbf{p}. \tag{14}$$

Upon substituting Eq. (14) in Eq. (12), the expression for $\delta\boldsymbol{\tau}$ in terms of the infinitesimal platform motion is obtained as:

$$\delta\boldsymbol{\tau} = \mathbf{K}_q\mathbf{J}\,\delta\mathbf{p}. \tag{15}$$

Thus, the second term on the right-hand side of Eq. (6) can be written as:

$$\mathbf{J}^T\,\delta\boldsymbol{\tau} = \mathbf{J}^T\,\mathbf{K}_q\mathbf{J}\,\delta\mathbf{p}. \tag{16}$$

For wire i, its stretch Δl_i under the effect of an axial load F_i is calculated as:

$$\Delta l_i = \frac{F_i(l_i + l_{ci})}{E_i A_{wi}}, \tag{17}$$

where $l_i + l_{ci}$ is the total length of wire i for a given position of the mobile platform; E_i is its equivalent Young's modulus of elasticity; $A_{wi} = \pi d_i^2/4$ is its cross-sectional area, and d_i is its nominal diameter. The stiffness of wire i, k_i, which varies with the wire length, is formulated as:

$$k_i = \frac{E_i A_{wi}}{l_i + l_{ci}}. \tag{18}$$

As it is evident from Eq. (18), when the mobile platform, i.e. point $\mathbf{p}$, approaches anchor A_i for which $l_i \approx 0$ a positive finite value for l_{ci} will ensure a finite value for the wire stiffness k_i.

Then the complete form of the stiffness matrix of the manipulator is derived as:

$$\mathbf{K} = \begin{bmatrix} k_{11} & k_{12} \\ k_{21} & k_{22} \end{bmatrix} = \mathbf{J}^T \mathbf{K}_q \mathbf{J} + \left(\tau_1 \begin{bmatrix} \sin\alpha_1 & 0 & \dots & 0 \\ -\cos\alpha_1 & 0 & \dots & 0 \end{bmatrix} + \cdots + \tau_n \begin{bmatrix} 0 & \dots & 0 & \sin\alpha_n \\ 0 & \dots & 0 & -\cos\alpha_n \end{bmatrix} \right) \mathbf{A}\,, \quad (19)$$

$$k_{11} = \sum_n \frac{E_i A_{wi} \cos^2\alpha_i}{l_i + l_{ci}} + \sum_n \frac{\tau_i \sin^2\alpha_i}{l_i}\,, \quad (20)$$

$$k_{12} = k_{21} = \sum_n \frac{E_i A_{wi} \cos\alpha_i \sin\alpha_i}{l_i + l_{ci}} - \sum_n \frac{\tau_i \cos\alpha_i \sin\alpha_i}{l_i}\,, \quad (21)$$

$$k_{22} = \sum_n \frac{E_i A_{wi} \sin^2\alpha_i}{l_i + l_{ci}} + \sum_n \frac{\tau_i \cos^2\alpha_i}{l_i}\,. \quad (22)$$

It is noteworthy that the above formulations of the Jacobian and stiffness matrices are with respect to a reference frame that has its origin at $\mathbf{p}$ and the same orientation as that of the fixed frame $\Psi(X,Y)$. As well, because the point of application of the external force on the mobile platform (a point mass) is coincident with the origin of this reference frame, as it is evident from Eqs. (19–22), this stiffness matrix is symmetric. Having the expressions for the entries of the stiffness matrix, this matrix can be calculated for every position of the mobile platform inside the workspace in order to develop the stiffness maps.

2.2. Single-dimensional stiffness

The single-dimensional stiffness is defined as the ratio of the 2-norm squared of the wrench $\mathbf{F}$ and the projection of $\mathbf{F}$ onto the direction along which the stiffness is sought. In [14], this index was formulated using the response $\delta\mathbf{p}$ in the direction of $\mathbf{F}$ (projection of $\delta\mathbf{p}$ onto the direction of $\mathbf{F}$) as $K_{sd} = \frac{\mathbf{F}^T\mathbf{F}}{\delta\mathbf{p}^T\mathbf{F}}$, in terms of the eigenvalues and eigenvectors of the symmetric positive definite matrix $\mathbf{J}^T\mathbf{K}_q\mathbf{J}$, the joint stiffness was treated as constant and the change in the Jacobian matrix under applied load was not included in the stiffness model. A similar index can be defined in terms of the eigenvalues and eigenvectors of the stiffness matrix of Eq. (19) as:

$$K_{sd} = \frac{\sum_{i=1}^{2} h_i \eta_i \boldsymbol{\rho}_i^T \sum_{i=1}^{2} h_i \eta_i \boldsymbol{\rho}_i}{\sum_{i=1}^{2} \eta_i \boldsymbol{\rho}_i^T \sum_{i=1}^{2} h_i \eta_i \boldsymbol{\rho}_i}\,, \quad (23)$$

where the ith eigenvalue and eigenvector of the stiffness matrix are denoted by h_i and $\boldsymbol{\rho}_i$, respectively. Scalar $\eta_i = \boldsymbol{\xi}.\boldsymbol{\rho}_i$ is the projection of vector $\boldsymbol{\xi}$, the direction in which the single-dimensional stiffness is calculated, onto eigenvector $\boldsymbol{\rho}_i$. It is noteworthy that for the planar translational (2 DOF) manipulators, vector $\mathbf{F}$ is unit consistent (all entries have the unit of Newtons), and hence, there is no need for a weighting matrix in Eq. (23).

An alternate index could be defined when the applied load is in X or Y direction. Using Eq. (7), when the applied load is in X direction, i.e. $F_y - mg = 0$, the stiffness in X direction is $k_x = k_{11} - \left(\frac{k_{12}^2}{k_{22}}\right)$; and when it is in Y direction, i.e. $F_x = 0$, $k_y = k_{22} - \left(\frac{k_{12}^2}{k_{11}}\right)$.

2.3. Failure of a wire

When wire i is disconnected or slack its contribution to the wrench of the mobile platform will be zero. After this type of failure, the corresponding ith entry of wire tensions vector $\boldsymbol{\tau}$, as well as the ith column of

the transposed Jacobian matrix of Eq. (4) and ith row of matrix $\mathbf{A}$ of Eq. (10) are eliminated. For example, when wire i fails, the reduced $(n-1)\times 1$ wire tension vector will be $\boldsymbol{\tau}_f = [\tau_1 \ \cdots \ \tau_{i-1} \ \tau_{i+1} \cdots \ \tau_n]^T$.

3. CASE STUDY

The wire-actuated parallel manipulator of Fig. 1, with three wires to provide translations along X and Y directions, is studied in this section. The wire tensions are formulated using Eq. (5) for a scalar λ as:

$$\tau_1 = \frac{\{2\cos\alpha_1-\cos(\alpha_1-2\alpha_2)-\cos(\alpha_1-2\alpha_3)\}F_x+\{2\sin\alpha_1+\sin(\alpha_1-2\alpha_2)+\sin(\alpha_1-2\alpha_3)\}(F_y-mg)}{\cos(2[\alpha_1-\alpha_2])+\cos(2[\alpha_1-\alpha_3])+\cos(2[\alpha_2-\alpha_3])-3} - \lambda\frac{\sin(\alpha_2-\alpha_3)}{\sin(\alpha_1-\alpha_2)}, \quad (24)$$

$$\tau_2 = \frac{\{2\cos\alpha_2-\cos(\alpha_2-2\alpha_2)-\cos(\alpha_2-2\alpha_3)\}F_x+\{2\sin\alpha_2+\sin(\alpha_2-2\alpha_1)+\sin(\alpha_2-2\alpha_3)\}(F_y-mg)}{\cos(2[\alpha_1-\alpha_2])+\cos(2[\alpha_1-\alpha_3])+\cos(2[\alpha_2-\alpha_3])-3} - \lambda\frac{\sin(\alpha_1-\alpha_3)}{\sin(\alpha_1-\alpha_2)}, \quad (25)$$

$$\tau_3 = \frac{\{2\cos\alpha_3-\cos(\alpha_3-2\alpha_2)-\cos(\alpha_3-2\alpha_1)\}F_x+\{2\sin\alpha_3+\sin(\alpha_3-2\alpha_2)+\sin(\alpha_3-2\alpha_1)\}(F_y-mg)}{\cos(2[\alpha_1-\alpha_2])+\cos(2[\alpha_1-\alpha_3])+\cos(2[\alpha_2-\alpha_3])-3} + \lambda. \quad (26)$$

To find the feasible region of λ, with positive wire tension, each wire tension is set to its minimum and maximum allowable values, τ_{min} and τ_{max}, i.e. $\tau_{\min} \le \tau_i \le \tau_{\min}$ for $i = 1,\cdots,3$, to calculate the minimum and maximum values of λ for each wire. The intersection of the three feasible regions for the three wires is the feasible region of λ for the manipulator. Inside the workspace of the manipulator, this feasible region of λ exists, i.e. $\lambda_{min}<\lambda_{max}$. Outside the workspace of the manipulator, the feasible region of λ does not exist and there is no λ to keep the tension of the three wires in the allowable tension limits. On the boundaries of the workspace, the feasible region of λ reduces to one point, i.e. $\lambda_{min} = \lambda_{max}$.

After failure of a wire, the 2×3 transposed Jacobian matrix reduces to a 2×2 square matrix $\mathbf{J}_f^T$ and the tension of the remaining wires is calculated using $\boldsymbol{\tau} = \mathbf{J}_f^{-T}\mathbf{F}$. For example, when wire 1 is slack, the tensions of wires 2 and 3 are calculated as:

$$\begin{bmatrix} \tau_2 \\ \tau_3 \end{bmatrix} = \mathbf{J}_f^{-T}\mathbf{F} = \begin{bmatrix} \frac{\sin\alpha_3 F_x-\cos\alpha_3(F_y-mg)}{\sin(\alpha_2-\alpha_3)} \\ -\frac{\sin\alpha_2 F_x-\cos\alpha_2(F_y-mg)}{\sin(\alpha_2-\alpha_3)} \end{bmatrix}. \quad (27)$$

The workspace of the manipulator after failure is formulated considering the wire tension limit of $\tau_{min} \le \tau_i \le \tau_{max}$ using the following inequalities:

$$\tau_{\min} \le \frac{\sin\alpha_3 F_x - \cos\alpha_3 (F_y - mg)}{\sin(\alpha_2-\alpha_3)} \le \tau_{\max}, \quad (28)$$

$$\tau_{\min} \le -\frac{\sin\alpha_2 F_x - \cos\alpha_2 (F_y - mg)}{\sin(\alpha_2-\alpha_3)} \le \tau_{\max}. \quad (29)$$

After failure, the stiffness matrix is derived using the formulations of Section 2 for $\boldsymbol{\tau}_f$, $\mathbf{J}_f$ and $\mathbf{A}_f$, for every position of the platform inside the workspace.

3.1. Stiffness Maps

The stiffness matrix of the three-wire manipulator shown in Fig. 1 is derived before and after the failure, and the corresponding single dimensional stiffness is formulated using Eq. (23) over the manipulator workspace. For $\boldsymbol{\xi} = [1 \ 0]^T$ and $\boldsymbol{\xi} = [0 \ 1]^T$, the single dimensional stiffness will be referred to as stiffness in "X direction" and "Y direction", respectively. The positions inside the workspace for which the desired minimum stiffness is achieved and the pertinent stiffness are identified and plotted. These plots are referred to as the stiffness maps in this paper. The manipulator is considered to move on the vertical plane (with gravity), whereas the gravitational force could be modelled as a 4^{th} wire with constant tension and acting in vertical direction. The anchor points A_i can move on a circular rail shown by dashed-line in Fig. 1 with

a radius of $0A_i = 1$ m and centered at the origin of the coordinate system $\Psi(X,Y)$ at point 0. For the stiffness maps developed in this subsection, the coordinates of anchors in terms of their angular positions for a radius of 1 meter are {285°, 45°, 165°}, i.e. the anchor positions of {(0.2588, −0.9659), (0.7071, 0.7071), (−0.9659, 0.2588)} meters are used. The anchor positions can be modified by moving on the circular rail, to identify the optimum layout of the manipulator.

In the simulations, the total constant mass of mobile platform and payload is $m = 2$ kg. For the wire actuators, 7×7 wire rope with a diameter of $d = 0.0015$ m and $E = 57.3$ GPa, manufactured from AISI 316 Stainless Steel grade 1.4401, is considered [15]. The minimum and maximum allowable wire tensions are set to 5 N and 500 N, respectively. The wire length between the motor spool and the pulley is fixed at $l_{ci} = 0.3$ m for all three wires. A modular motor-pulley assembly, which could be mounted at any orientation with respect to the circular rail, would allow a constant value for l_{ci} when the anchor positions are adjusted.

Before wire failure, as long as the manipulator is within its wrench closure workspace and the conditions for positive tension are satisfied [12], in general there are infinite possible solutions for the wire tensions within the acceptable range of λ. Thus, among possible solutions, the solution corresponding to λ_{max} using Eq. (5) is chosen and used in the stiffness map calculations in this section. This results in maximum possible tension for wires (with appropriate safety factor), while satisfying the force balance equations and maximum stiffness for every position of the mobile platform. Thus, this selection will result in the largest stiffness maps for a required minimum stiffness.

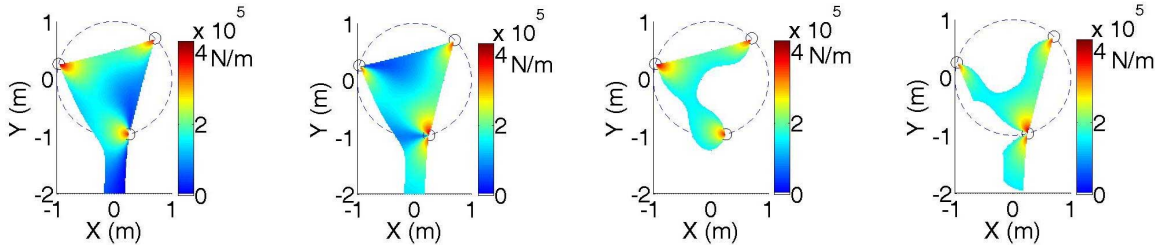

(a) along X direction (b) along Y direction (c) along X direction (d) along Y direction

Fig. 2. Stiffness maps for a minimum stiffness K_{min} of: (a), (b) 0 KN/m; (c), (d) 150 KN/m.

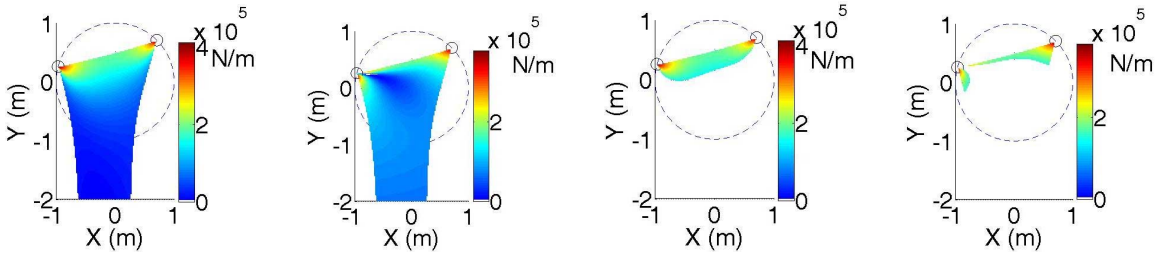

(a) along X direction (b) along Y direction (c) along X direction (d) along Y direction

Fig. 3. Stiffness maps after failure of wire 1 for K_{min} of: (a), (b) 0 KN/m; (c), (d) 150 KN/m.

Plots of Fig. 2 show the stiffness maps along the X and Y directions, when the only external force applied on the mobile platform is gravity. Anchor positions are marked with small circles in the plots. Stiffness maps of the manipulator for the required minimum stiffness $K_{\min}$ of 0 and 150 kN/m are shown in Figs. 2 (a,b) and 2 (c,d), respectively. For a minimum stiffness of 150 kN/m, the corresponding deflection for a payload of 150 N is 0.001 m, which is a reasonable positioning accuracy for an assembly task using a manipulator

of this size. Comparing the plots of Figs. 2 (a,b) with Figs. 2 (c,d), it is verified that for a given layout of manipulator, the stiffness map for a higher value of the required minimum stiffness is a sub-region of the map for zero minimum stiffness.

Figure 3 depicts the stiffness maps after failure of wire 1 for a required minimum stiffness of 0 and 150 kN/m, respectively. Comparing plots of Figs. 2 (a,b) with Figs. 3 (a,b), it is clear that the stiffness maps after failure of wire 1 are larger than the maps before failure. This is because of the selected tension limits of $\tau_{\min} = 5$N, $\tau_{\max} = 500$ N and the required minimum stiffness of zero. For example, at position $\mathbf{p} = [-0.5 \;\; -1.0]^T$ of Figs. 2 (a,b), the tension of wire 1 is $\tau_1 = 2.813 \leq \tau_{\min} = 5$ N, respectively, while the other two wires fulfill the tension limits. Hence this position is not in the stiffness map of Figs. 2 (a,b). It is noteworthy that at this position of manipulator, after failure of wire 1, the tension limits are satisfied with the remaining two wires and the gravitational force of $mg = 19.6$ N. With a higher value for the required minimum stiffness, comparing Figs. 2 (c,d) with Figs. 3 (c,d), it can be seen that the stiffness maps shrink drastically after failure.

3.2. Optimum layouts of manipulator

In this section, anchor positions of the manipulator are optimized to maximize the stiffness map area. In other words, the optimum layout of the manipulator is identified to maximize the workspace with the required minimum stiffness, considering the constraint that the anchor positions should be on the circular rail shown in Fig. 1. The stiffness maps for the optimum layouts of the manipulator are developed, with the required minimum stiffness, before and after failure. The wire tension constraints are checked for each potential position of mobile platform to identify the workspace before and after failure. For all the positions of the platform inside the workspace, the stiffness matrix is derived following the procedure discussed in Section 2. After deriving the stiffness map, the number of positions inside the map corresponds to the area of the stiffness map (workspace area with the desired minimum stiffness). This integer number of positions is converted to an estimate of the area knowing that the increment of 0.02 m for positions in X and Y directions is considered.

To identify the optimum anchor positions that maximize the stiffness map area, the *genetic algorithm* (GA) of MATLAB is used. In the optimization, the number of anchor positions (population size) for each population is set to 20, where the array of anchor positions (solution to the optimization problem) is the population. At each iteration, the current populations are used to produce a new population (new generation). The number of generations, which is the maximum number of iterations before the algorithm halts, is set to 100. The algorithm runs until the cumulative change in the fitness function value over the last 50 generations is less than 10^{-6}. The next generation is made of the anchor positions that are guaranteed to survive from the previous generation (elite children) and the anchor positions made by crossover. The migration fraction is set to 0.2 to allow the best anchor position from one subpopulation replace the worst one in another subpopulation. The crossover fraction is 0.8, which specifies the fraction of the next generation, other than elite children that are produced by crossover (combining two anchor positions, or parents, to form a crossover position for the next generation). An initial penalty parameter of 10 is used to eliminate the anchor positions that violate the constraints, and the penalty parameter is increased by a penalty factor of 100 when the problem is not solved to the required accuracy and the constraints are not satisfied.

In this optimization problem, the goal is to maximize the stiffness map area with the constraint that the anchor positions should be on a circular rail with the radius of 1 m and centered at point 0. The optimum anchor positions for the manipulator before failure and when the mobile platform is under the effect of gravity have been identified as {(0.9999, 0.0048), (−0.9984, −0.0566), (−0.0334, 0.9994)}. The stiffness maps for this optimum layout are shown in the plots of Figs. 4 (a-b), with the optimum stiffness map area of 3.3502 m^2. The whole number values for the anchor positions, i.e. {(1, 0), (−1, 0), (0, 1)}, have also

been checked but this would result in a slightly smaller stiffness map area of 3.3438 m^2. In calculating and comparing these values of the stiffness map areas, the finer resolution of 0.005 m in generating the positions in X and Y directions is considered. The optimum anchor positions for the manipulator before failure for the required minimum stiffness of 150 kN/m have been identified as {(−0.4524, −0.8918), (−0.9991, 0.0423), (0.9788, 0.2049) } for the stiffness along X direction and {(−0.2476, −0.9689), (0.9397, 0.3421), (−0.1050, 0.9945)} for the stiffness along Y direction, with the corresponding stiffness maps shown in Figs. 4 (c,d). Comparing the plots of Figs. 4 (a,b) with Figs. 4 (c,d), it is evident that, unlike the plots of Fig. 2, for different required minimum stiffness, the optimum layouts and the variation of stiffness within the identified workspace are different. Optimum anchor positions for the case that the stiffness in both X and Y directions are over 150 kN/m are {(− 0.9939, − 0.1100), (0.9999, 0.0119), (0.0707, 0.9975)}, with the corresponding stiffness maps shown in Fig. 5.

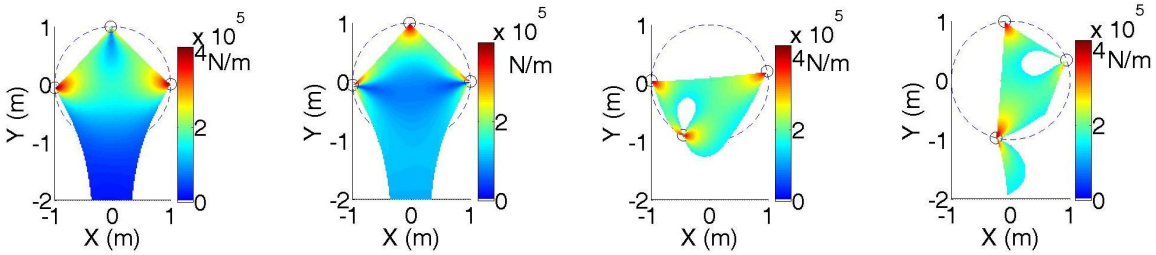

(a) along X direction (b) along Y direction (c) along X direction (d) along Y direction

Fig. 4. Stiffness maps with optimum layout for K_{min} of: (a), (b) 0 KN/m; (c), (d) 150 KN/m.

(a) along X direction (b) along Y direction

Fig. 5. Stiffness maps with optimum layout for $K_{min} = 150$ KN/m in both X and Y directions.

When a wire fails the optimum positions of the remaining two anchors do not depend on which wire fails as long as the wires have the same properties. The optimum anchor positions for the manipulator after failure of a wire have been identified as {(−0.9769, 0.2135), (0.9819, 0.1892)}, with the corresponding stiffness maps shown in Figs. 6 (a,b) and the optimum stiffness map area of 3.2013 m^2. The notch in Fig. 6 (b), close to the center of circular rail, is due to color mapping of stiffness with smaller order of magnitude. The whole number values for the anchor positions, i.e. {(−1, 0), (1, 0)}, would result in a slightly smaller stiffness map area of 3.0433 m^2. The optimum anchor positions for the minimum stiffness of 150 kN/m after failure of a wire have been identified as {(−0.9960, 0.0897), (0.9974, 0.0717)} for the stiffness along X direction and {(−0.0114, 0.9999), (0.9999, 0.0017)} for the stiffness along Y direction. Similar to the previous cases, the whole number values for the anchor positions would result in slightly smaller stiffness map areas. Thus, the optimum anchor positions are used and the stiffness maps for these optimum layouts are shown in Figs. 6 (c,d). Considering the plots of Fig. 6 it is demonstrated that after a wire failure, the optimum layouts and the variation of stiffness within the identified workspace are completely different

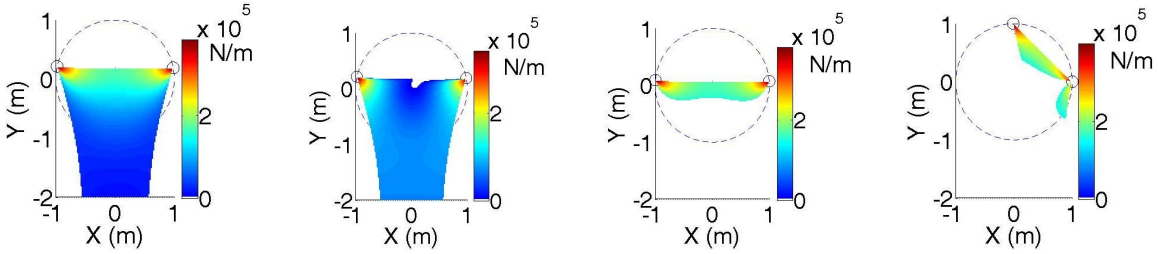

(a) along X direction (b) along Y direction (c) along X direction (d) along Y direction

Fig. 6. Stiffness maps with optimum layout after failure of a wire for K_{min} of: (a), (b) 0 KN/m; (c), (d) 150 KN/m.

(a) along X direction (b) along Y direction

Fig. 7. Stiffness maps with optimum layout after failure of a wire for $K_{min} = 150$ KN/m in both X and Y directions.

for a higher required minimum stiffness compared to the zero minimum stiffness case. Optimum anchor positions for the case that the stiffness in both X and Y directions are over 150 kN/m are $\{(-0.3699, 0.9291), (0.9999, 0.0047)\}$, with the corresponding stiffness maps shown in Fig. 7. Comparing the stiffness maps before and after optimization, it can be seen that the area of the stiffness maps have been increased after optimizing the layout of the manipulator.

4. DISCUSSION AND CONCLUSIONS

In this article, the complete form of the stiffness matrix of planar translational wire-actuated parallel manipulators was formulated parametrically. Using the differential form of the static force balance equations, the variation of wire stiffness with wire length and the change in the Jacobian matrix under external loading were included in the stiffness model. The effects of the wire tension limits, required minimum stiffness, manipulator layout, as well as wire failure on the workspace of manipulators and their stiffness were studied. The positions inside the workspace that satisfy the wire tension limits, as well as the required minimum stiffness, were considered to develop the stiffness maps of manipulators. The stiffness characteristics of a three-wire-actuated manipulator were investigated and the single-dimensional stiffness maps before and after a wire failure were developed. Optimum wire anchor positions to maximize the area of the stiffness maps were identified and the corresponding stiffness maps were developed. The optimum layouts can be used when designing the manipulators, as well as for their control in order to retrieve the lost stiffness after wire/actuator failure and to achieve a better fault tolerant manipulator.

REFERENCES

1. Dagalakis, N.G., Albus, J.S., Wang, B.-L., Unger, J. and Lee, J.D., "Stiffness study of a parallel link robot crane for shipbuilding applications", *Journal of Offshore Mechanics and Arctic Engineering*, Vol. 111, pp. 183–193, 1989.
2. Sahin, S. and Notash, L., "Force and stiffness analysis of wire-actuated parallel manipulators", *Proceedings of 12th World Congress in Mechanism and Machine Science*, 2007.
3. Pigoski, T., Griffis, M. and Duffy, J., "Stiffness mappings employing different frames of reference", *Mechanism and Machine Theory*, Vol. 33, No. 6, pp. 825–838, 1998.
4. Chen, S. and Kao, I., "Conservative congruence transformation for joint and Cartesian stiffness matrices of robotic hands and fingers", *International Journal of Robotics Research*, Vol. 19, No. 9, pp. 835–847, 2000.
5. Griffis, M. and Duffy, J., "Global stiffness modeling of a class of simple compliant couplings", *Mechanism and Machine Theory*, Vol. 6, No. 2, pp. 207–224, 1993.
6. Zefran, M. and Kumar, V., "Affine connections for the Cartesian stiffness matrix", *Proceedings of IEEE Conference on Robotics and Automation*, pp. 1376–1381, 1997.
7. Kovecses, J. and Angeles, J.,"The stiffness matrix in elastically articulated rigid-body systems", *Multibody System Dynamics*, Vol. 18, No. 2, pp. 169–184, 2007.
8. Cho, W., Kino, H., Katsuta, K. and Kawamura, S., "A design of parallel wire driven robots for ultrahigh speed motion based on stiffness analysis", *Proceedings of Japan-USA Symposium on Flexible Automation*, Vol. 1, pp. 159–166. 1996.
9. Liu, X.J., Jin, Z.L. and Gao, F., "Optimum design of 3-DOF spherical parallel manipulators with respect to the conditioning and stiffness indices", *Mechanism and Machine Theory*, Vol. 35, No. 9, pp. 1257–1267, 2000.
10. Azadi, M., Behzadipour, S. and Faulkner, G., "Antagonistic variable stiffness elements", *Mechanism and Machine Theory*, Vol. 44, No. 9, pp. 1746–1758, 2009.
11. Notash, L. and Huang, L., "On the design of fault tolerant parallel manipulators", *Mechanism and Machine Theory*, Vol. 38, No. 1, pp. 85–101, 2003.
12. Notash, L., "Failure recovery for wrench capability of wire-actuated parallel manipulators", *Robotica*, Vol. 30, No. 6, pp. 941–950, 2012.
13. Moradi, A. and Notash, L., "Investigation of wire failure effect on stiffness maps of planar wire-actuated parallel manipulators", *Proceedings of ASME 34th Annual Mechanisms and Robotics Conference (IDETC/CIE 2010)*, 2010.
14. El-Khasawneh, B.S. and Ferreira, P.M., "Computation of stiffness and stiffness bounds for parallel link manipulators", *International Journal of Machine Tools & Manufacture*, Vol. 39, No. 2, pp. 321–342, 1999.
15. S3i Ltd., http://www.s3i.co.uk/wire-rope-technical.php, accessed April 2012.